Emission of white-light in cubic $Y_4Zr_3O_{12}$:Yb^{3+} induced by a continuous infrared laser

Federico González[a,b,*], Rabindra Khadka[a], Rigoberto López-Juárez[c], John Collins[d], Baldassare Di Bartolo[a]

[a] *Department of Physics, Boston College, 02467 Chestnut Hill, MA, USA*
[b] *Departamento de Ingeniería de Procesos e Hidráulica, Universidad Autónoma Metropolitana-Iztapalapa, A.P. 55-534, 09340 Ciudad de México, Mexico*
[c] *Unidad Morelia del Instituto de Investigaciones en Materiales, Universidad Nacional Autónoma de México, Antigua Carretera a Pátzcuaro No. 8701, Col. Ex Hacienda de San José de la Huerta, C.P. 58190 Morelia, Michoacán, Mexico*
[d] *Department of Physics, Wheaton College, 02766 Norton, MA, USA*

ARTICLE INFO

ABSTRACT

In this work nanostructured powders with nominal composition $Y_4Zr_3O_{12}$, undoped and doped at Yb^{3+} 1 mol%, were synthesized by the polymerizable complex method. The crystal structure, microstructure and performance to produce white-light continuous emission spectra of powders under 975 nm continuous laser irradiation were investigated by X-ray diffraction (XRD), scanning electron microscopy (SEM), high resolution transmission electron microscopy (HRTEM), and optical spectroscopy. Continuous emission spectra of white-light were well-fitted by Planck's law of blackbody radiation. The threshold power values for generating white-light in sample annealed at 800 °C and 1100 °C were 1.36 W and 1.75 W, respectively. This difference was attributed to the crystallite size. The dependence of the absolute temperature, obtained from Planck's law fittings, as a function of the laser's power is explained as due to the microstructural changes, verified by XRD measurements. Finally, a stimulating mechanism of white-light generation involving non-radiative processes of Yb^{3+} is suggested.

1. Introduction

The generation of white-light (WL) in nanostructured materials undoped and doped with lanthanides using infrared lasers, has been a subject of different research studies. The materials investigated comprise semiconductors (e.g silicon) [1,2], carbon nanotubes [3], graphene foam [4,5], and SiC [1]. Perhaps the most widely studied systems to exhibit broadband WL emission are insulating oxide hosts, both doped and undoped, where the materials are almost always nano-powders. The undoped oxides in which WL has been observed include, for example, YAG and GGG [6], and Y_2O_3 [7], γ-$Y_2Si_2O_7$ [8], and Al_2O_3 [9]. Oxide systems partially-doped with rare earth and transition metal ions in which WL emission has been observed include the following: La_2O_3 doped with Er^{3+} and Yb^{3+} [10]; Yb^{3+}-doped ZrO_2 [11]; Ln-doped YVO_4 (Ln^{3+} = Er^{3+}, Tm^{3+}, Ho^{3+}) [12]; Yb-doped YAG [13]; Y_2O_3 doped with trivalent lanthanides such as Nd [14], Yb [15,16] and Er [16]; γ-$Y_2Si_2O_7$ doped with Yb^{3+} [9]; and GGG [6]; and (Gd, Er, Yb)$_2O_3$ attached to gold nanorods [17]. Finally, white light has been observed in several oxides containing lanthanides ions in stoichiometric concentrations, including $NdAlO_3$ [18], $LiYbP4O12$ [19], Er_2O_3 [9,20],

$Yb_3Al_5O_{12}$ [21], Yb_2O_3 [21,22], Sm_2O_3 and Tm_2O_3 [22] and Nd_2O_3/gold composites [23].

Noticeably, many of the above insulating materials where WL has been observed contain Yb^{3+}. This is likely because the absorption of Yb^{3+} is resonant with diode lasers near 980 nm, which can produce high power. Thus, the presence of Yb^{3+} allows for absorption of the photons from the IR laser, which helps lead to the WL emission. In several researches works there is a lack of the details about the exact shape of the emission spectra, as there was little information as to whether the spectra were corrected or not, which makes comparisons difficult. In those works that have reported corrected data, there is strong evidence supporting thermal radiation as the origin of the WL generation [5,11]. However, other mechanisms originating WL have also been proposed such as multiphoton excitation followed by emission [2,4,7,8,12]. In any case, the exact mechanisms by which Yb absorptions lead to WL emission are unclear.

In order to gain additional insight about the origin of the WL generation, it could be of interest to investigate this phenomenon in samples of the ZrO_2-Y_2O_3 solid-solution, designated in general as yttria stabilized zirconia (YSZ). YSZ's possess remarkable physical properties,

---

making them suitable for a wide range of technological applications such as thermal barrier coatings [24,25] and electrolytes in solid oxide fuel cells [26]. Moreover, one of the most interesting characteristic of YSZ is its low thermal conductivity, which results from the chemical disorder induced when Zr^{4+} is replaced by Y^{3+} [27]. The cubic like-fluorite phase is strongly stabilized relative to monoclinic and tetragonal phases of ZrO2 by the addition of Y^{3+}, and dissolves up to about 70 mol% Y^{3+} [28]. At around 57 mol% Y^{3+} it has been confirmed the $Y_4Zr_3O_{12}$ intermediary phase, with nominal composition $Y_4Zr_3O_{12}$, with an ordered fluorite structure [29,30].

Among YSZ systems, in none of its compositions, except in ZrO2: Yb^{3+}, has been reported the generation of WL by the infrared laser irradiation [11].

To ascertain if a YSZ compound and whether Yb^{3+} and crystallite size may have any effect on generation of continuous white-light under laser irradiation, in this work, we synthesized $Y_4Zr_3O_{12}$ undoped and doped at Yb^{3+} 1 mol% having different crystallite size in the nanometric scale and irradiated them with a 975 nm laser. Finally, emission spectra observed were analyzed using the Plank's law.

2. Experimental

Polymerizable complex method was used for the synthesis of $Y_4Zr_3O_{12}$ and $Y_{3.93}Yb_{0.07}Zr_3O_{12}$, hereafter referred as YZO and YZOYb. The raw materials used were yttrium(III) nitrate hexahydrate (99.8%), zirconium(IV) oxynitrate hydrate (99%), ytterbium(III) nitrate penta-hydrate (99.9%), citric acid, ethylene glycol and deionized water. An aqueous solution was prepared by dissolving the required amounts of zirconium oxynitrate, yttrium and ytterbium nitrates. This solution was stirred for 30 min, then citric acid and ethylene glycol were added. The solution was kept at 70 °C for evaporating the excess water and to produce a viscous solution. For promoting polymerization, the temperature was set at 90 °C until a solid resin was formed. The resin was then transferred to an oven for a heat treatment at 350 °C for 30 min. After that, the pre-calcined powders were heat treated at 800 °C for 1 h. Then, powders were calcined again at 1100 °C for 1 h.

The X-ray diffractograms (XRD) of the samples were measured in air at room temperature using a Bruker D-8 Advance diffractometer with the Bragg-Brentano θ-θ geometry, Cu Kα radiation, a Ni 0.5% Cu–Kβ filter in the secondary beam, and a one-dimensional position-sensitive silicon strip detector (Bruker, Lynxeye). The diffraction intensity as a function of 2θ angle was measured between 15° and 105°, with a 2θ step of 0.020415°, for 76.8 s per point. Crystalline structures were refined using the Rietveld method by using the fundamental parameters approach [31] during the refinements, as implemented in the TOPAS Academic code, version 6. The parameters used in refinements included polynomial terms for modeling of the background, the lattice parameters, terms indicating the position and intensity of the "tube tails", specimen displacement, structural parameters, and the width of a Lorentzian profile for modeling the average crystallite size. This last feature was modeled in reciprocal space with a symmetrized harmonics expansion [32]. The standard deviations, given in parentheses in the text, show the variation in the last digit of a number; when they correspond to Rietveld refined parameters. The morphology of powders was observed by field emission scanning electron microscopy in a JEOL7600F electron microscope. High resolution transmission electron microscopy (HRTEM) was performed in a JEOL microscope model JEM-ARM200F.

Emission spectra were recorded in the range from 425 nm to 880 nm at room temperature and at a pressure of 0.5 Pa with an Ocean Optics USB4000 spectrometer fitted with a 3648-element linear silicon CCD array detector. The excitation source of light was provided by the laser diode power supply LDI-820 coupled with a diode laser emitting at 975 nm. A 900 nm short-pass filter was employed to block the signal of the laser. Samples were mounted in a Janis Research cryostat model RD, which was evacuated to attain the low pressure. The spectra were
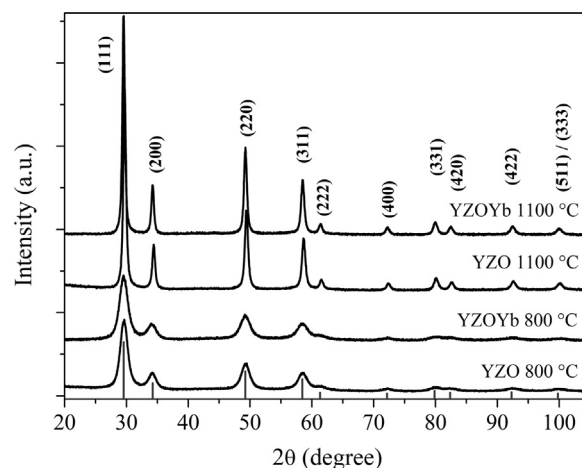

Fig. 1. X-ray diffraction patterns of sample YZO and YZOYb annealed at 800 °C and 1100 °C for 1 h. The vertical lines correspond to the adapted reference pattern PDF-30-1468. Miller indices of planes associated with each maximum are given on the top.

corrected for the wavelength dependent response of the spectrometer/detector system.

3. Results and discussion

In Fig. 1 are shown the X-ray diffraction patterns of powders of YZO undoped and doped with Yb^{3+}. All the diffraction peaks match well with those corresponding to the cubic like-fluorite crystal phase of ZrO_2 (PDF-30-1468) when it is stabilized with concentrations higher than 15 mol% of Y^{3+} [28]. The only noticeable difference among the XRD patterns is the width of the peaks, associated with different crystal size: broader for samples annealed at 800 °C as compared with those ones annealed at 1100 °C, i.e., smaller crystal size obtained at lower annealing temperature, as expected. In order to quantify the average crystallite size, and the cell parameter as function of composition and annealing temperature, the XRD patterns were analyzed by the Rietveld refinement method. The unit cell of the zirconia fluorite-type structure, was modeled with the cubic symmetry described by the *Fm-3m* space group, and a basis containing one Zr^{4+} and one O^{2-} at the relative coordinates (0, 0, 0), and (1/4, 1/4, 1/4), respectively The initial cubic cell parameter was approximated in terms of the molar composition *w* in the formula $Zr_{1-w}Y_wO_{2-w/2}$ from the linear equation *a = 0.200w + 5.1063* [33], except that in this case, *w* represents the sum of mole fractions of Y^{3+} and Yb^{3+}. The Y^{3+} and Yb^{3+} were set at Zr^{4+} site. Occupancy of ions was fixed in accordance with the stoichiometry given by the formulae $Y_4Zr_3O_{12}$ and $Y_{3.93}Yb_{0.07}Zr_3O_{12}$.

To compare experimental X-ray diffractograms with the calculated ones, Rietveld refinement plots of sample YZOYb annealed at 800 °C and 1100 °C are depicted in Fig. 2. The figure of merit (R_{wp}) for these fits are given in Table 1, and show excellent agreement between experimental and calculated data. Table 1 also shows the average crystallite size, and the cell parameter obtained from the Rietveld refinement analyses. As it is noticed from data in Table 1, the cubic cell parameter seems to be insensitive, at the uncertainty level of the Rietveld analysis, to the incorporation of Yb^{3+}, but not to the annealing temperature. The first fact may be due to the small difference between the ionic radii of Y^{3+} and Yb^{3+}. According to Shannon [34], in an VIII-coordination as that present in the fluorite-like structure, the ionic radii of Y^{3+} and Yb^{3+} are 1.019 Å and 0.985 Å, respectively. Average crystallite size for all specimens are in the nanometric scale. However, it is more than three times larger for samples annealed at 1100 °C than for samples annealed at 800 °C; furthermore, the addition of Yb^{3+} also promotes a reduction of the crystallite size.

Given that crystallite size, morphology and composition could play an important role in the performance of the materials to produce WL,
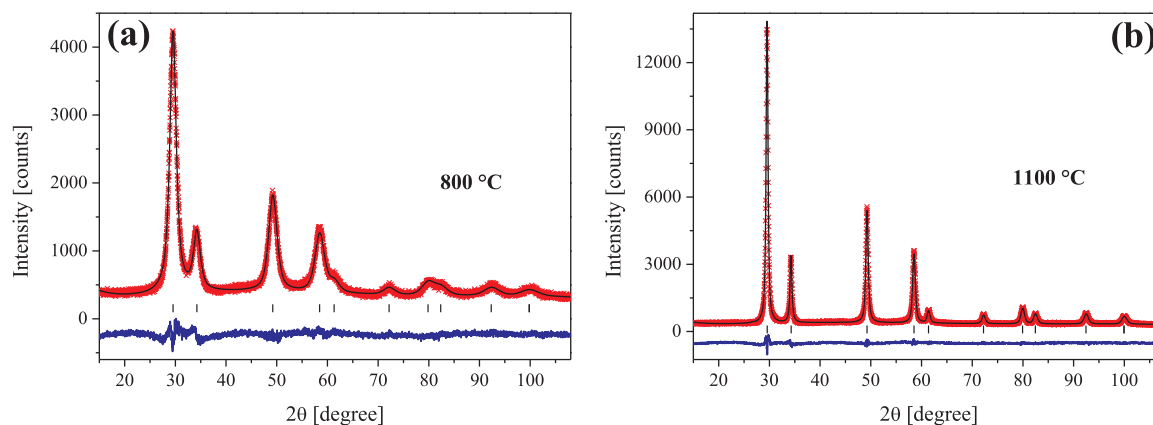
Fig. 2. Rietveld refinement plot of the sample YZOYb annealed at 800 °C (a) and 1100 °C (b). The scatter crosses and the upper solid line correspond to the experimental and calculated data, respectively. The lower curve in each plot is the difference between calculated and measured diffraction patterns. Marks on the bottom represent the Bragg reflections associated with the cubic fluorite-like crystal phase.

Table 1
Lattice parameter, average crystallite size and R_{wp} of YZO and YZOYb annealed at 800 °C and 1100 °C.

Sample	Annealing temperature (°C)	a (Å)	Average crystallite size (nm)	R_{wp}
YZO	800	5.2346(8)	8.4(1)	5.66
YZO	1100	5.2277(1)	30.2(1)	4.93
YZOYb	800	5.2322(11)	7.4(1)	6.05
YZOYb	1100	5.2274(3)	25.8(1)	5.73

SEM and HRTEM studies were carried out to get information about the morphology and the crystallite size of our samples. In Fig. 3(a) and (b) are shown images of the YZOYb sample annealed at 800 °C and 1100 °C, respectively. In the micrographs are observed agglomerates of crystallites. The morphology of both samples seems similar despite the difference in the annealing temperature. Although the average crystallite size cannot be measured exactly from these images, the sizes are smaller than 100 nm being compatible with those values obtained from the Rietveld analyses. However, HRTEM images can provide the appropriate information about the crystallite size and the crystal structure at the local scale. In Fig. 4, are presented some representative images of sample YZOYb annealed at 800 °C (Fig. 4(a)) and at 1100 °C (Fig. 4(b)). From these images, it is also evident the nanometric size of the crystallites, despite the synthesis method makes difficult to de-agglomerate them. The scale in both images, is in accordance with the average crystallite size calculated from the Rietveld refinement, confirming at more local level the enlargement of crystallite sizes due to the increase in the annealing temperature. Regarding the crystal structures, Fig. 4(c) shows an image of the sample annealed at 1100 °C along the [111] zone

axis and its respective periodic ion arrangement within the nanocrystal. If both images in this figure are looked in detail, the good agreement between them is clearly seen.

Irradiation by the 975 nm laser generates WL emission in a persistent way only in the sample containing Yb^{3+}, while the undoped sample exhibited only ephemeral WL production, thus making its characterization impractical. Fig. 5 shows the emission spectra of YZOYb sample annealed at 800 °C (Fig. 5(a)) and 1100 °C (Fig. 5(b)) for different laser powers as well as representative images of the WL emitted by both samples. As it is observed, the intensity of emission increases as the wavelength increases, and similarly an increase in the integrated intensity of the emitted WL is observed as the laser irradiation increases. The sudden dropping in signal at 890 nm is due to the cut-off filter employed for blocking the laser signal. For the data shown in Fig. 5(c) (800 °C) and (d) (1100 °C), the spectra are taken consecutively, first starting at low laser power and increasing the power up to 5.55 W, and then decreasing the laser power. It seems, that after the sample is exposed to the laser at the maximum power (5.55 W), the material likely undergoes some modification because the emission intensity, for the same powers when decreasing the laser power, is reduced as compared when going up. This hysteresis effect, similar to one previously reported [15], is more noticeable for sample annealed at 800 °C.

Following the approach reported in [5,11] we fit our spectra using the Planck's law of blackbody radiation given by the expression $I(\lambda, T) = a \frac{2\pi h c^2}{\lambda^5 (\exp(\frac{hc}{\lambda kT}) - 1)}$ (see Fig. 6), where T is the absolute temperature of the blackbody, λ is wavelength, a is a fitting parameter related with the view factor [35], which is the proportion of the radiation which leaves the surface of the sample and strikes the detector, h is the
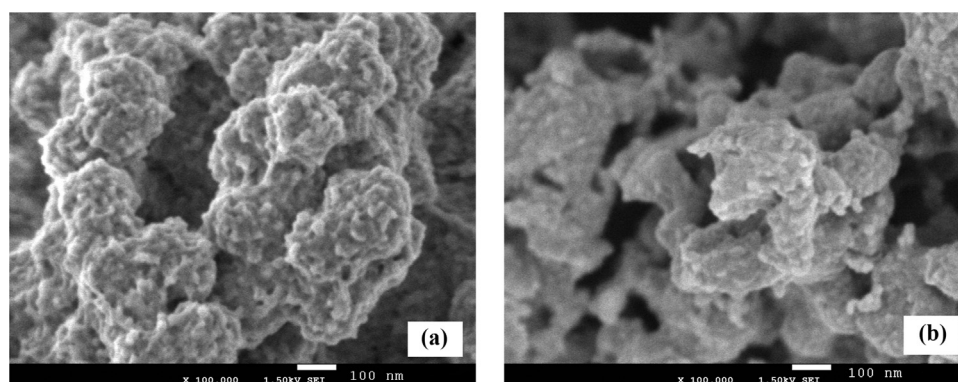

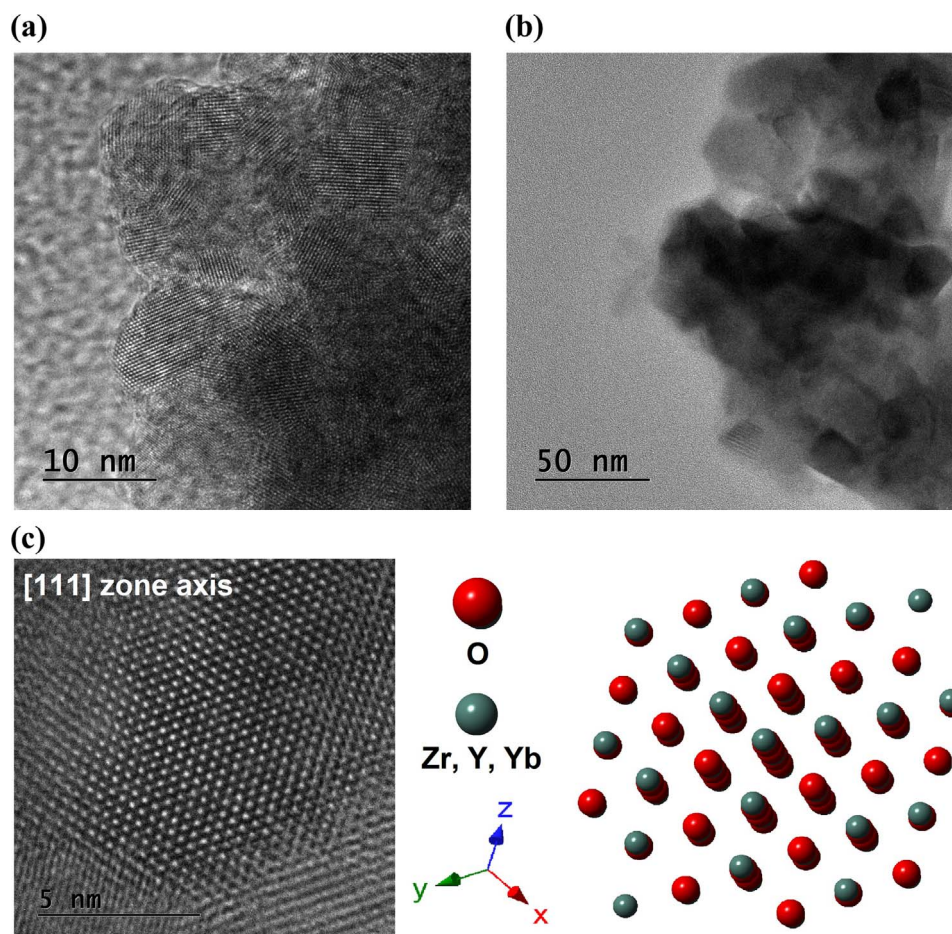**Fig. 3.** SEM images of YZOYb annealed at 800 °C (a), and 1100 °C (b).

Fig. 4. HRTEM images of sample YZOYb annealed at 800 °C (a), 1100 °C (b). Notice the difference in the scale between (a) and (b). In (c) is shown the image from a thin crystal of sample annealed at 1100 °C along [111] zone axis (left) and its ion arrangement (right). It is clearly seen the agreement between both.

Planck constant, c is the speed of light, and k is the Boltzmann constant.

An important data resulting from Plank's law fitting of the emission spectra is the absolute temperature of the sample surface, irradiated by the laser. In Fig. 7 the temperatures obtained from fittings of sample YZOYb annealed at 800 °C and 1100 °C, are plotted as a function of the laser power. In the inset of Fig. 7 are depicted the chromaticity color coordinates CIE 1931 calculated from some emission spectra for different laser powers, and they match well with the corresponding Planckian locus in that diagram at their respective temperatures.

Interesting to notice, is the different behavior in the temperature as a function of the laser power for both samples, depending on the annealing temperature. The power thresholds for WL generation are around 1.36 W and 1.75 W for annealing at 800 °C and 1100 °C, respectively. This fact is attributed to the differences in the thermal conductivities associated with the average crystallite size. In a previous report, reducing crystallite size to 30 nm was found to have little effect on the measured values of the thermal conductivity [36]. On the other hand, Soyez et al. [37] have found a significant reduction in thermal conductivity when crystallite size was reduced to around 10 nm. Thus, it would be expected substantial differences between samples annealed at 800° and 1100 °C when exposed to the laser radiation, because as reported in Table 1, their average crystallite sizes are 7.4 nm and 25.8 nm. Less power is needed to increase the temperature in sample with smaller crystallites, since conductive losses of heat would be lower.

Also intriguing in Fig. 7 is the temperature dependence of the sample annealed at 800 °C; the temperature increases up to a maximum at ∼ 2190 K, followed by a decrease in its value. We propose this change is due to the enlargement of the crystallites at the very localized

zone where laser power is falling on the sample. This enlargement would result in a higher thermal conductivity at a local level, leading to the spread of the "hot zone" where WL is generated, explaining in this way why the temperature is lower, but the integrated intensity increases, as noticed in Fig. 5(b). The temperature of sample annealed at 1100 °C increases if the irradiance does the same. From the power threshold, up to 3.00 W, the temperature increases quickly, but then a linear trend is observed up to 8.00 W, the maximum value we could reach in our experimental setup. In this sample, a more stable microstructure is expected since this sample was heat treated at higher temperature. However, it is not possible to rule out some microstructural changes in the zone irradiated by the laser, because although the melting temperature of our compound is greater than 2750 K [28], the temperatures reached are between 400 K and 800 K higher than those ones used for annealing this sample. Moreover, despite the sample YZOYb annealed at 800 °C and 1100 °C, reach these high temperatures, any macroscopic evidence of the degradation of the sample is observed after laser irradiation.

Above, we proposed that the emission intensity of the 800 °C sample reaching a maximum and then decreasing as the laser power increases (see Fig. 7) is due to the enlargement of the crystallite size under laser irradiation. To test this hypothesis, we performed X-ray diffraction measurements on the sample YZOYb annealed at 800 °C and 1100 °C before and after it was irradiated with the laser at 3.21 W for 30 min; these are representative conditions of the laser power and elapsed time during our experiments. Certainly, this measurement represents, in a way, a challenge because the spot of the laser is around 1 mm in diameter, very small in comparison with the size of the X-ray beam. To overcome this problem, and be able to observe noticeable changes, we
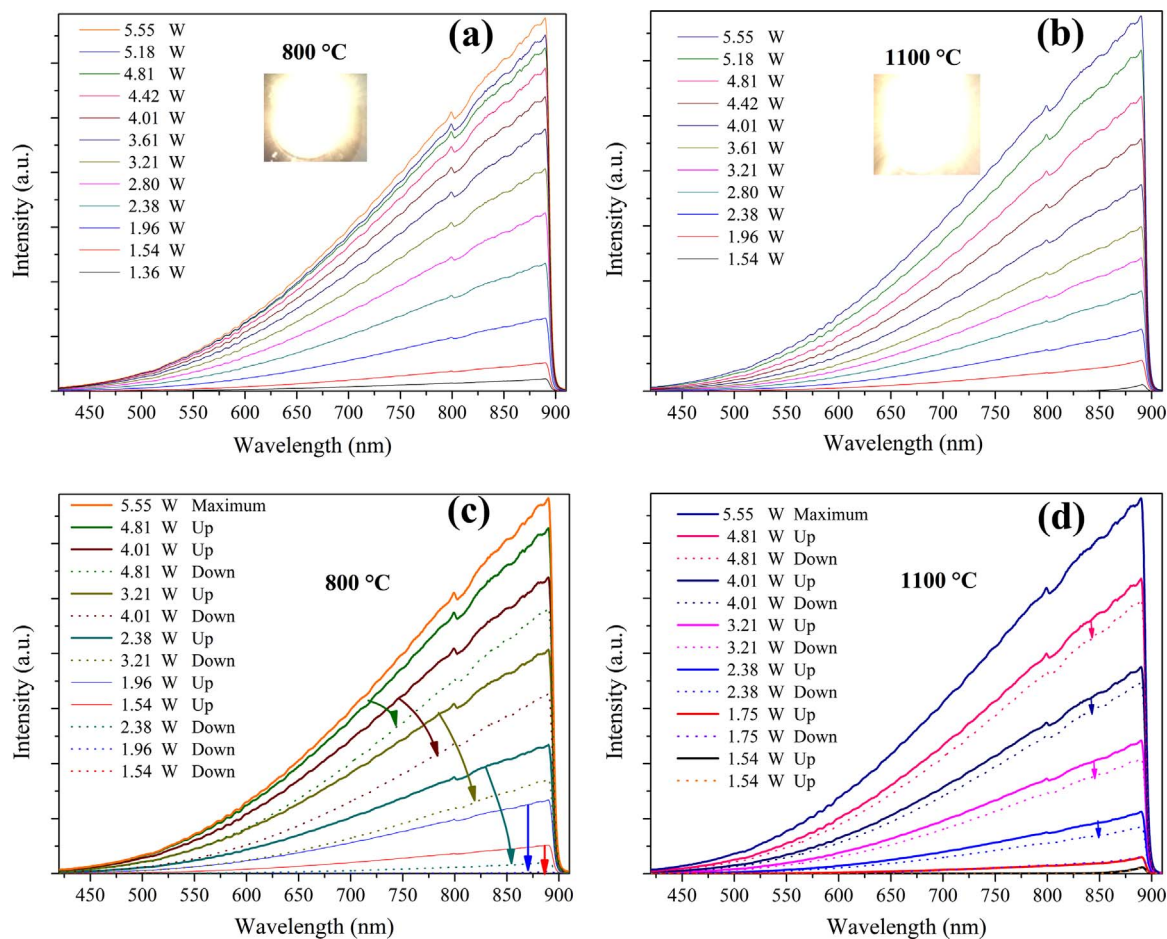
Fig. 5. Emission spectra of sample YZOYb annealed at 800 °C ((a), (c)), and 1100 °C ((b), (d)) for different laser powers. In (a) and (b) the laser power was changed from lower to higher values; while in figures (c) and (d) the laser power was first increased until reaching a maximum and then decreased until the light emission disappeared. In the insets of (a) and (b), pictures of white-light produced by both samples are shown.

used small amounts of sample to have comparable areas between the total area scrutinized by the X-rays and that one exposed to the laser. In Fig. 8 are depicted the X-ray diffraction patterns, before and after laser irradiation, of the sample YZOYb annealed at 800 °C and 1100 °C. Also shown in the figure is the background, which has an important contribution to the X-ray patterns due to the small area exposed by the sample in comparison with the whole area of the sample holder exposed to the X-ray beam.

The effects of the laser irradiation on the microstructure of the sample annealed at 800 °C are evident; their manifestations are the increase in the intensity of the diffraction maxima and their respective narrowing. These observations are compatible with the enlargement of the crystallites. On the other hand, the pattern of the sample annealed at 1100 °C does not exhibit any evident change after being exposed to the laser (for the verticals shifts see caption of Fig. 8). Thus, some evolution happens in the evidently less stable sample annealed at lower
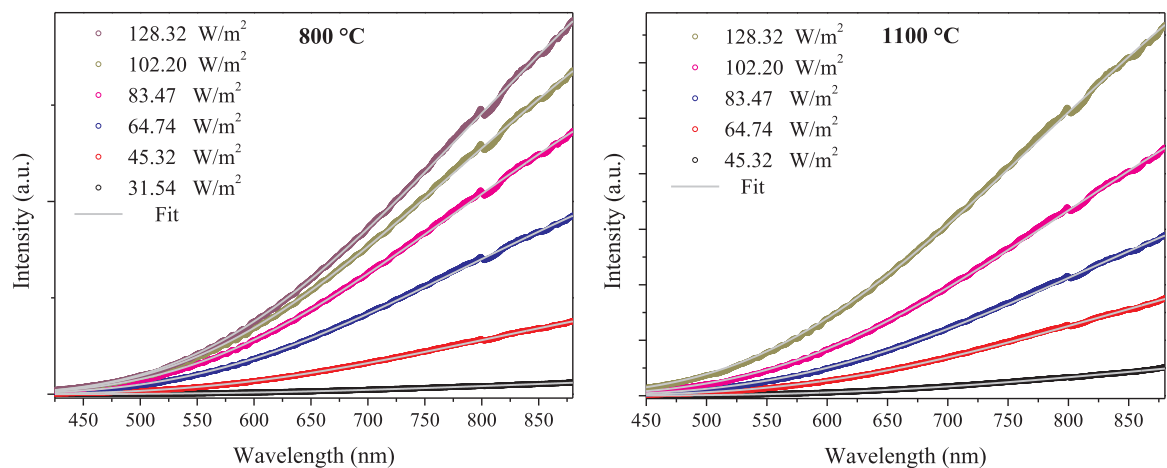

Fig. 6. Representative emission spectra of sample YZOYb annealed at 800 °C (a), and 1100 °C (b) for different laser powers and their corresponding Planck's law blackbody radiation fitting.
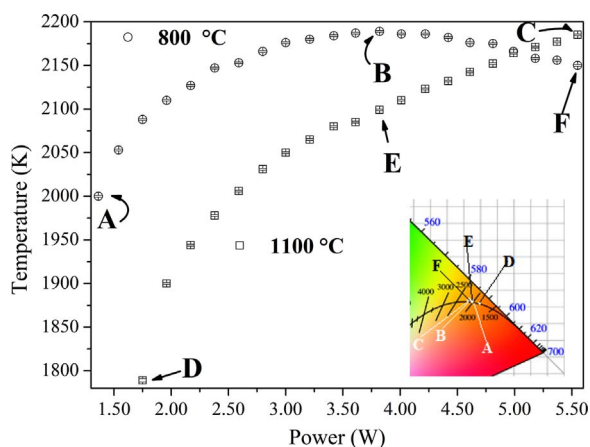
Fig. 7. Temperature as a function of laser power for sample YZOYb annealed at 800 °C and 1100 °C. In the inset is shown a portion of the color space CIE 1931, where the color coordinates corresponding to representative temperatures (A to F) obtained from Plank's law fittings of emission spectra are plotted. The continuous curve in black into the CIE diagram corresponds to the Planckian locus and represents the path in the space color of a blackbody as the blackbody temperature (also indicated) changes.
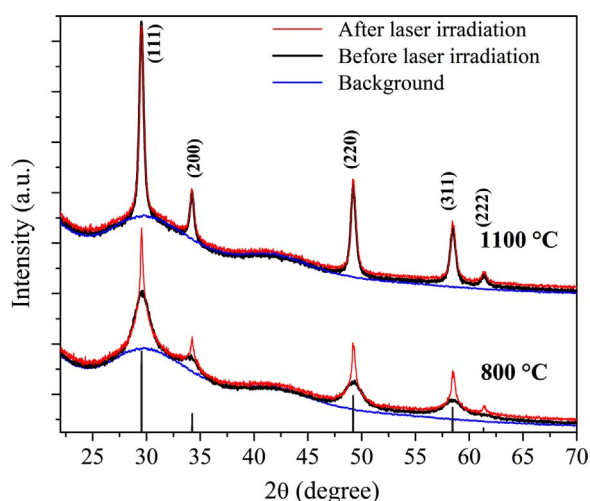

Fig. 8. XRD patterns, before and after laser irradiation (3.21 W and 30 min) of sample YZOYb annealed at 800 °C and 1100 °C. For each annealing temperature, the order of the pattern is as follows: the lower corresponds to the background, the middle corresponds to the sample before it is irradiated, and the upper corresponds to the sample after it is irradiated. The small vertical shifts between the patterns before and after irradiation, were incorporated by us for the sake of clarity. Also, are showed the positions of the XRD maxima according to PDF- PDF-30-1468. Miller indices of planes associated with each maximum are given on the top.

temperature. This fact strongly supports the previous ideas about the behavior seen in Fig. 7.

Although the XRD pattern of the sample annealed at 800 °C exposed to the laser shows significantly changes, it is also important to note that the modification of the crystallite size must occur only in the specific point where the laser hits the powder, because sharp maxima coexist at the same time with broad peaks, almost identical to those of the sample before it is irradiated with the laser, and in our opinion produced by the X-ray diffraction in those areas not exposed to the laser. This detail, which may seem minor, could provide insight into the region in which the laser is heating the sample, and therefore the region where white-light is "produced".

Despite the previous results, it remains open the question about why there are differences in the emission intensity at the same laser intensity depending on whether the laser power is being increased or decreased. We hypostatize this could be due to subtler microstructural changes, because in sample annealed at 1100 °C no evident modifications are
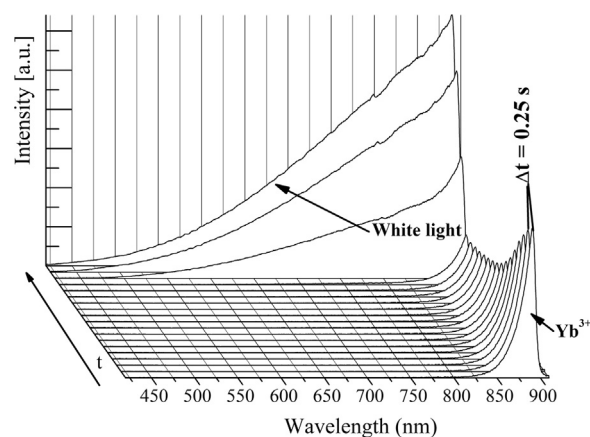

Fig. 9. Selected emission spectra (of a larger series), illustrating the emission behavior of the sample YZOYb annealed at 1100 °C and irradiated under a laser power of 5.18 W, 4 s before WL emission starts. Band on the right, corresponds to Yb^{3+} emission.

noticed by the XRD measurement, even when the emission intensity at a certain laser power was different when going up and going down in power.

Regarding the role of Yb^{3+} in the generation of WL, we have found very interesting results due to the experimental set up we used to perform the emission spectra measurement. Since the spectro-photometer used can obtain the emission intensity over a wide wavelength interval at the same time, we were able to record many spectra in a short period of time. We used this feature to monitor the emission from the sample just prior to the generation of white light. For this purpose, an integration time of 100 ms was selected, and a time of 250 ms elapsed between each measuring. In the Fig. 9, some selected spectra of a larger series of them are depicted, and it shows the emission behavior of sample YZOYb annealed at 1100 °C four seconds before the sample starts to emit WL. At early times, we observe a single emission band in the 850–900 nm region. We ascribed this incomplete (because the 900 nm cut-off filter) emission band in the long wavelength region of the spectra to Yb^{3+}. This result is also supported by the fact that such band was not observed in the undoped sample, but only in the doped one, even at irradiances far below the threshold needed for WL generation. It is seen in Fig. 9 that as the time increases, the Yb^{3+} emission diminishes continuously. After that, the tail at the shorter wavelengths, i.e. white-light region, suddenly appears, and after 0.50 s the WL emission becomes stable. The behavior depicted in Fig. 9, seems to explain, at least for samples containing Yb^{3+}, the role of this ion in stimulating the WL generation. The absorption of the laser is efficient because it matches the energy difference between the levels $^2F_{7/2}$ and $^2F_{5/2}$ of Yb^{3+}. Then, since non-radiative processes are always present, the system gains energy and increase its temperature in a such way that the non-radiative processes become dominant leading to the quenching of the Yb^{3+} emission, and to an abrupt increase in the temperature of the system which produce the continuous emission of light. Alternatively, the emission of Yb^{3+} could be also decreasing due to excited state absorption from Yb ions to other (defect) centers in the solid, which may decay nonradiatively.

4. Conclusions

Powders of $Y_4Zr_3O_{12}$ and $Y_{3.93}Yb_{0.07}Zr_3O_{12}$ were synthesized by the polymerizable complex method. Crystallite size, in the nanometric scale, was tuned by changing the annealing temperature. The samples exhibit a cubic fluorite- like crystal structure. The average crystallite sizes of sample $Y_{3.93}Yb_{0.07}Zr_3O_{12}$ estimated by Rietveld analysis were 7.4 nm and 25.8 nm for samples annealed at 800 °C and 1100 °C. Confirmation of the crystallite size was done by HRTEM. Sustained white-light emission under 975 nm laser irradiation was only observed

for sample doped with Yb^{3+}. Emission spectra of the white-light were successfully fitted by Planck's law of blackbody radiation, and the absolute temperatures as a function of the laser irradiation resulting from fittings were explained in terms of the expected thermal conductivity. Furthermore, the dependence of the absolute temperature as a function of the laser irradiation was explained as due to the microstructural changes, and then verified by XRD measurements. Also, the hysteresis of the emission intensity depending on whether the laser power is increasing or decreasing could be related to the microstructural changes, though in the sample annealed at 1100 °C are subtler; no changes were noticed by XRD measurements between the irradiated and non-irradiated samples annealed at 1100 °C. Calculated color coordinates (CIE 1931) from emission spectra agreed well with their corresponding temperatures in the Planckian locus. Finally, we explain a possible mechanism which favors the white-light generation when Yb^{3+} is present in the samples.

Acknowledgments

References

[1] P. Roura, J. Costa, M. López-de Miguel, B. Garrido, J. Fort, J.R. Morante, E. Bertran, Black-body emission from nanostructured materials, J. Lumin. 80 (1998) 519–522.

[2] D.P. Savin, Y.O. Roizin, D.A. Demchencko, Properties of laser ablated porous silicon, Appl. Phys. Lett. 69 (96) (1996) 3048.

[3] Z.H. Lim, A. Lee, Y. Zhu, K.Y. Lim, C.H. Sow, Sustained laser induced incandescence in carbon nanotubes for rapid localized heating, Appl. Phys. Lett. 94 (2009) 073106.

[4] W. Strek, R. Tomala, M. Lukaszewicz, B. Cichy, Y. Gerasymchuk, P. Gluchowski, L. Marciniak, A. Bednarkiewicz, D. Hreniak, Laser induced white-lighting of graphene foam, Sci. Rep. 7 (2017) 41281.

[5] W. Strek, B. Cichy, L. Radosinski, P. Gluchowski, L. Marciniak, L. Marciniak, L. Lucascewicz, D. Hreniak, Laser induced white-lighting of graphene – opening a band gap in graphene, Light: Sci. Appl. 4 (2015) e237, http://dx.doi.org/10.1038/lsa.2015.10.

[6] G. Bilir, G. Ozen, M. Bettinelli, F. Piccinelli, M. Cesaria, B. Di Bartolo, Broadband visible light emission from nominally undoped and Cr^{3+} doped garnet nanopowders, IEEE Photonics J. 6 (2014) 2201211.

[7] G. Bilir, B. Di Bartolo, Production of bright, wideband white-light from Y_2O_3 nanopowders induced by laser diode emission, Opt. Mater. 36 (2014) 1357–1360.

[8] M. Erdem, G. Eryurek, B. DiBartolo, White light emission from sol–gel derived γ-$Y_2Si_2O_7$ nanoparticles, J. Alloy. Compd. 639 (5) (2015) 483–487.

[9] S. Tabanli, H. Cinkaya Yilmaz, G. Bilir, M. Erdem, G. Eryurek, B. Di Bartolo, J. Collins, Broadband white light emission from doped and undoped insulators, ECS J. Solid State Sci. 7 (1) (2018) R3199–R3210.

[10] A.K. Singh, S. Singh, D. Kumar, D.K. Rai, S.B. Rai, K. Kumar, Light-into-heat conversion in La_2O_3:Er^{3+}-Yb^{3+} phosphor: an incandescent emission, Opt. Lett. 37 (2012) 776–778.

[11] J. Wang, T. Ming, Z. Jin, J. Wang, L.D. Sun, C.H. Yan, Photon energy upconversion through thermal radiation with the power efficiency reaching 16%, Nat. Commun. 5 (2014) 5669.

[12] Y. Zhu, W. Xu, C. Li, H. Zhang, B. Dong, L. Xu, S. Xu, H. Song, Broad white-light and infrared emission bands in YVO_4: Yb^{3+}, Ln^{3+} (Ln^{3+} = Er^{3+}, Tm^{3+}, or Ho^{3+}), Appl. Phys. Express 5 (2012) 092701.

[13] W. Strek, L. Marciniak, P. Gluchowski, D. Hreniak, Infrared laser stimulated broadband white emission of Yb:YAG nanoceramics, Opt. Mater. 35 (2013) 2013–2017.

[14] G. Bilir, J. Ozen, M. Collins, Cesaria, B. Di Bartolo, Unconventional production of bright white light emission by Nd-doped and nominally undoped Y_2O_3 nanopowders, IEEE Photonics J. 6 (4) (2014) 8200518.

[15] S.M. Redmond, S.C. Rand, S.L. Oliveira, Bistable emission of a black-body radiator, Appl. Phys. Lett. 85 (2004) 5517–5519.

[16] S.M. Redmond, S.C. Rand, X.L. Ruan, M. Kaviany, Multiple scattering and nonlinear thermal emission of Yb^{3+} and Er^{3+}:Y_2O_3 nanopowders, J. Appl. Phys. 95 (8) (2004) 4067–4077.

[17] M.L. Debasu, D. Ananias, I. Pastoriza-Santos, L.M. Liz-Marzán, J. Rocha, L.D. Carlos, All-in-one optical heater-thermometer nanoplatform operative from 300 to 2000 K based on Er^{3+} emission and blackbody radiation, Adv. Mater. 25 (2013) 4868–4874.

[18] W. Strek, L. Marciniak, D. Hreniak, A. Lukowiak, Anti-Stokes bright yellowish emission from $NdAlO_3$ nanocrystals, J. Appl. Phys. 111 (2012) 024305.

[19] W. Strek, L. Marciniak, A. Bednarkiewicz, A. Lukowiak, R. Wiglusz, D. Hreniak, White emission of lithium ytterbium tetraphosphate nanocrystals, Opt. Express 19 (2011) 14083.

[20] J. Wang, J.H. Hao, P. Tanner, Persistent luminescence upconversion for Er_2O_3 under 975 nm excitation in vacuum, J. Lumin. 164 (2015) 116–122.

[21] J. Wang, J.H. Hao, P. Tanner, Luminous and tunable upconversion for YAG (Yb3Al5O12) and (Yb,Y)2O3 nanopowders, Opt. Lett. 35 (23) (2010) 3922–3924.

[22] J. Wang, P.A. Tanner, Upconversion for white-light generation by a single compound, J. Am. Chem. Soc. 132 (2010) 947–9490.

[23] X. Chen, W. Xu, Y. Zhu, P. Zhou, S. Cui, L. Tao, L. Xua, H. Song, Nd_2O_3/Au nanocomposites: upconversion broadband emission and enhancement under near-infrared light excitation, J. Mater. Chem. C 2 (2014) 5857–5863.

[24] D.R. Clarke, S.R. Phillpot, Thermal barrier coating materials, Mater. Today 8 (2005) 22–29.

[25] X.Q. Cao, R. Vassen, D. Stoever, Ceramic materials for thermal barrier coatings, J. Eur. Ceram. Soc. 24 (2004) 1–10.

[26] N. Mahato, A. Banerjee, A. Gupta, S. Omar, K. Balani, Progress in material selection for solid oxide fuel cell technology: a review, Prog. Mater. Sci. 72 (2015) 141–337.

[27] P.K. Schelling, S.R. Phillpot, Mechanism of thermal transport in zirconia and yttria-stabilized zirconia by molecular-dynamics simulation, J. Am. Ceram. Soc. 84 (2001) 2997–3007.

[28] M. Chen, B. Hallstedt, L.J. Gauckler, Thermodynamic modeling of the ZrO_2–$YO_{1.5}$ system, Solid State Ion. 170 (2004) 255–274.

[29] H.G. Scott, The yttria-zirconia-phase, Acta Crystallogr. B33 (1977) 281–282.

[30] S.P. Ray, V.S. Stubican, Fluorite related ordered compounds in the ZrO_2-CaO and ZrO_2-Y_2O_3 systems, Mater. Res. Bull. 12 (1977) 549–556.

[31] R.W. Cheary, A.A. Coelho, A fundamental parameters approach to X-ray line-profile fitting, J. Appl. Crystallogr. 25 (1992) 109–121.

[32] M. Järvinen, Application of symmetrized harmonics expansion to correction of the preferred orientation effect, J. Appl. Crystallogr. 26 (1993) 525–531.

[33] M. Yashima, N. Ishizawa, M. Yoshimura, Application of an ion-packing model based on defect clusters to zirconia solid solutions: II, applicability of Vegard's law, J. Am. Ceram. Soc. 75 (1992) 1550–1557.

[34] R.D. Shannon, Revised effective ionic radii and systematic studies of interatomic distances in halides and chalcogenides, Acta Crystallogr. A32 (1976) 751–767.

[35] M.F. Modest, Radiative Heat Transfer, second ed., Academic Press, San Diego, 2003.

[36] S.R. Raghavan, H. Wang, R.B. Dinwiddie, W.D. Porter, M.J. Mayo, The effect of grain size, porosity, and yttria content on the thermal conductivity of nanocrystalline zirconia, Scr. Mater. 39 (1998) 1119–1125.

[37] G. Soyez, J.A. Eastman, L.J. Thompson, R.J. DiMelfi, G.-R. Bai, P.M. Baldo, A.W. McCormick, A.A. Elmustafa, M.F. Tambwe, D.S. Stone, Grain-size- dependent thermal conductivity of nanocrystalline yttria-stabilized zirconia films grown by metal-organic chemical vapor deposition, Appl. Phys. Lett. 77 (2000) 1155–1157.